Chapter 5
Finite Element Approach for Composite Magneto-Piezoelectric Materials Modeling in ACELAN-COMPOS Package

Natalia V. Kurbatova, Dmitry K. Nadolin, Andrey V. Nasedkin, Pavel A. Oganesyan, and Arcady N. Soloviev

Abstract The problem of material properties identification for modern active composites is closely connected to the state of the art methods of design and manufacturing using composite and smart materials. This chapter deals with computer design of multiscale two-phase piezomagnetoelectric (magnetoelectric) bulk composites in finite element software ACELAN-COMPOS. These composites consist of piezomagnetic and piezoelectric fractions of irregular structures. The complex approach for the homogenization problem of such composites include the effective moduli method, computer modeling of the representative volumes with microstructure features, and the finite element technologies for solving the static problems for the representative volumes. Representative volumes are widely used as geometrical models for such problems. The three-dimensional application is demonstrated for piezomagnetoelectric and piezoelectric materials. A specific set of boundary conditions applied to the representative volume enables us to determine effective moduli of the material. The first step of such modeling consists in describing a material distribution inside the representative volumes with a known percentage of each material. Three algorithms were created to simulate random material distribution for specific patterns: biphasic composite with connectivity of each phase, granules of predefined size and regular rods.

Natalia V. Kurbatova, Dmitry K. Nadolin, Andrey V. Nasedkin, Pavel A. Oganesyan
Southern Federal University, Institute of Mathematics, Mechanics and Computer Science, Milchakova Street 8a, Rostov-on-Don, 344090, Russia
e-mail: nvk-ru@yandex.ru,nadolin@yandex.ru,nasedkin@math.sfedu.ru,wolwerine@yandex.ru

Arcady N. Soloviev
Don State Technical University, Department of Theoretical and Applied Mechanics, Gagarin sq., 1, Rostov-on-Don, 344000, Russia
e-mail: solovievarc@gmail.com

H. Altenbach et al. (eds.), *Analysis and Modelling of Advanced Structures and Smart Systems*, Advanced Structured Materials 81,
https://doi.org/10.1007/978-981-10-6895-9_5

5.1 Introduction

Inhomogeneous and porous active materials are widely used in modern material science and technique. Thus, two-phase piezomagnetoelectric (magnetoelectric) composites consisting of active piezoelectric and piezomagnetic phases demonstrate the ability to mutual transformation of magnetic and electric fields, although each separate phase does not have such property. Modern magnetoelectric composites have high effectiveness of the magnetoelectric transformation, relatively high temperatures of phase transitions and long process life (Nan et al, 2008).

Piezoceramic composite materials and, in particular, porous piezoceramic materials also have been actively developed in the last years (Ringgaard et al, 2015; Rybyanets, 2010, 2011). Porous piezoceramics have a lower impedance than dense ceramics. Therefore, the impedance mismatch between the piezoelectric device and the surrounding acoustic medium is decreased. On the other hand, its longitudinal piezomodulus d_{33}, which determines the efficiency of mechanical and electrical energy transformations for thickness vibrations, remains almost the same as for the dense piezoceramics. This properties allows to create high-intensity ultrasound transducers.

Recently magnetoelectric composites became of interest to many researchers which resulted in considerable increase in the number of works devoted to the modeling of the effective properties of these composites (see Lee et al, 2005; Li, 2000; Nan et al, 2008; Tang and Yu, 2008; Zhang and Soh, 2005, etc.). Piezoelectric composites are studied much better (see Bowen et al, 2001; Iyer and Venkatesh, 2014; Martínez-Ayuso et al, 2017; Nguyen et al, 2016; Ramesh et al, 2005; Rybyanets, 2010; Rybyanets et al, 2015; Topolov and Bowen, 2009, etc.). Example of such materials can be seen in Figs. 5.1 and 5.2.

Mathematical models of such materials are complicated and usually require additional modeling step to define physical properties of composite. In this paper we consider homogenization models and the finite element method as a tool for

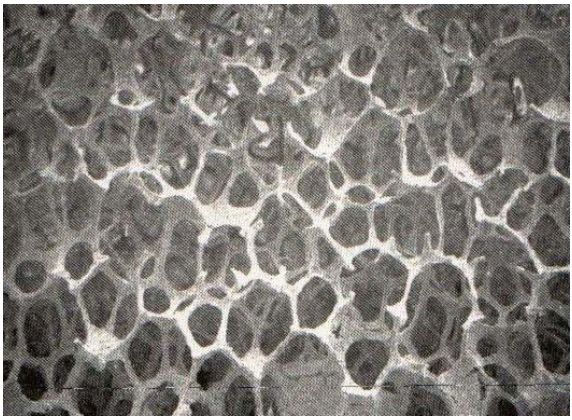

Fig. 5.1 Scanning electron microscope (SEM) picture of a high-porous PZT material with 95 % of porosity synthesized by foam reticulation technique.

Fig. 5.2: Piezoceramics with different size of pores and pores percentage.

representative volume modeling and properties identification of piezoelectric and magnetoelectric materials.

5.2 Piezomagnetoelectric Boundary Problems

In ACELAN we use the original models of piezomagnetoelectric (magnetoelectric) materials with damping similar described in Nasedkin et al (2014).

Let Ω be a region occupied by a piezomagnetoelectric material; $\Gamma = \partial\Omega$ is the boundary of the region; $\mathbf{n}$ is the vector of the external unit normal to Γ; $\mathbf{x} = \{x_1, x_2, x_3\}$; t is the time; $\mathbf{u} = \mathbf{u}(\mathbf{x}, t)$ is the vector of mechanical displacements; $\varphi = \varphi(\mathbf{x}, t)$ is the electric potential; $\phi = \phi(\mathbf{x}, t)$ is the magnetic potential. The system of differential equations for piezomagnetoelectric body with damping effects in Ω can be written in the following vector–matrix form

$$\mathbf{L}^*(\nabla)\cdot\mathbf{T} + \rho\mathbf{f} = \rho(\ddot{\mathbf{u}} + \alpha_d\dot{\mathbf{u}}), \quad \nabla\cdot\mathbf{D} = \sigma_\Omega, \quad \nabla\cdot\mathbf{B} = 0, \tag{5.1}$$

$$\mathbf{T} = \mathbf{c}\cdot(\mathbf{S} + \beta_d\dot{\mathbf{S}}) - \mathbf{e}^*\cdot\mathbf{E} - \mathbf{h}^*\cdot\mathbf{H}, \tag{5.2}$$

$$\mathbf{D} + \zeta_d\dot{\mathbf{D}} = \mathbf{e}\cdot(\mathbf{S} + \zeta_d\dot{\mathbf{S}}) + \boldsymbol{\kappa}\cdot\mathbf{E} + \boldsymbol{\alpha}\cdot\mathbf{H}, \tag{5.3}$$

$$\mathbf{B} + \gamma_d\dot{\mathbf{B}} = \mathbf{h}\cdot(\mathbf{S} + \gamma_d\dot{\mathbf{S}}) + \boldsymbol{\alpha}^*\cdot\mathbf{E} + \boldsymbol{\mu}\cdot\mathbf{H}, \tag{5.4}$$

$$\mathbf{S} = \mathbf{L}(\nabla)\cdot\mathbf{u}, \quad \mathbf{E} = -\nabla\varphi, \quad \mathbf{H} = -\nabla\phi, \tag{5.5}$$

$$\mathbf{L}^*(\nabla) = \begin{bmatrix} \partial_1 & 0 & 0 & 0 & \partial_3 & \partial_2 \\ 0 & \partial_2 & 0 & \partial_3 & 0 & \partial_1 \\ 0 & 0 & \partial_3 & \partial_2 & \partial_1 & 0 \end{bmatrix}. \tag{5.6}$$

Here $\mathbf{L}(\mathbf{a})$ is a matrix operator for the vector $\mathbf{a}$, $\mathbf{L}^*(\mathbf{a})$ is the transposed operator, $\mathbf{T} = \{\sigma_{11}, \sigma_{22}, \sigma_{33}, \sigma_{23}, \sigma_{13}, \sigma_{12}\}$ denotes the array of the stress components; $\mathbf{S} = \{\varepsilon_{11},$

ε_{22}, ε_{33}, $2\varepsilon_{23}$, $2\varepsilon_{13}$, $2\varepsilon_{12}\}$ is the array of the strain components; $\mathbf{D}$ and $\mathbf{E}$ are the electric flux density vector or the electric displacement vector and the electric field vector; $\mathbf{B}$ and $\mathbf{H}$ are the magnetic flux density vector and the magnetic field vector; ρ is the mass density of the material; $\mathbf{c} = \mathbf{c}^{E,H}$ is the 6×6 matrix of elastic stiffness moduli; $\mathbf{e} = \mathbf{e}^{H}$ is the 3×6 matrix of piezoelectric moduli; $\mathbf{h} = \mathbf{h}^{E}$ is the the 3×6 matrix of magnetostriction moduli (piezomagnetic moduli); $\boldsymbol{\kappa} = \boldsymbol{\kappa}^{S,H} = \boldsymbol{\varepsilon}^{S,H}$ is the the 3×3 matrix of dielectric permittivity moduli; $\boldsymbol{\alpha} = \boldsymbol{\alpha}^{S}$ is the 3×3 matrix of magnetoelectric coupling coefficients; $\boldsymbol{\mu} = \boldsymbol{\mu}^{S,E}$ is the 3×3 matrix of magnetic permeability moduli; α_d, β_d, ζ_d, γ_d are the damping coefficients; $\mathbf{f}$ is the vector of mass forces; σ_Ω is the density of free electric charges (usually, $\sigma_\Omega = 0$); $(...)^*$ is the transpose operation; $(...) : (...)$ is the double scalar product operation.

We suppose that the material moduli have the usual symmetry properties: $c_{\alpha\beta} = c_{\beta\alpha}$, $\kappa_{kl} = \kappa_{lk}$, $\mu_{kl} = \mu_{lk}$. In addition to this for the positive definiteness of the intrinsic energy for the piezomagnetoelectric medium the following inequalities must be satisfied ($\forall$ $\mathbf{S}$, $\mathbf{E}$, $\mathbf{H}$), $\exists W_0 > 0$:

$$\mathbf{S}^* \cdot \mathbf{c} \cdot \mathbf{S} + \mathbf{E}^* \cdot \boldsymbol{\kappa} \cdot \mathbf{E} + 2\mathbf{E}^* \cdot \boldsymbol{\alpha} \cdot \mathbf{H} + \mathbf{H}^* \cdot \boldsymbol{\mu} \cdot \mathbf{H} \geq W_0(\mathbf{S}^* \cdot \mathbf{S} + \mathbf{E}^* \cdot \mathbf{E} + \mathbf{H}^* \cdot \mathbf{H}).$$

In Eqs. (5.1)–(5.6) for the piezomagnetoelectric material, we use a generalized Rayleigh method of damping evaluation, see Belokon et al (2002); Nasedkin (2010) for the case of piezoelectric material and Nasedkin et al (2014) for the case of thermopiezomagnetoelectric material with equations in tensor form. When $\zeta_d = \gamma_d = 0$ in Eqs. (5.3), (5.4), we have the model for taking into account of mechanical damping in piezomagnetoelectric media which is adopted in the case of elastic and piezoelectric materials in several well-known finite element packages. A more complicated model (5.2)–(5.4) extends Kelvin's model to the case of piezomagnetoelectric media. It has been shown that the model (5.1)–(5.6) with $\beta_d = \zeta_d = \gamma_d$ satisfies the conditions of the energy dissipation and has the possibility to apply the mode superposition method for transient and harmonic problems.

The boundary and the initial conditions should be added to the system of differential equations (5.1)–(5.6). The boundary conditions are of three types: mechanical, electric and magnetic. To formulate the mechanical boundary conditions we assume that the boundary Γ is divided in two subsets Γ_σ and Γ_u ($\Gamma = \Gamma_\sigma \cup \Gamma_u$). We will assume that at the part of the boundary Γ_σ the vector of mechanical stress $\mathbf{p}_\Gamma$ is known

$$\mathbf{L}^*(\mathbf{n}) \cdot \mathbf{T} = \mathbf{p}_\Gamma, \qquad \mathbf{x} \in \Gamma_\sigma. \tag{5.7}$$

On the remaining part Γ_u of the boundary Γ we pose known the mechanical displacements vector $\mathbf{u}_\Gamma$

$$\mathbf{u} = \mathbf{u}_\Gamma, \quad \mathbf{x} \in \Gamma_u, \tag{5.8}$$

where $\mathbf{L}^*(\mathbf{n})$ is the matrix as in (5.6) with replace ∂_k by n_k. To set the electric boundary conditions we assume that the surface Γ is also subdivided in two subsets: Γ_D and Γ_φ ($\Gamma = \Gamma_D \cup \Gamma_\varphi$). The regions Γ_D does not contain electrodes and hold the following conditions

$$\mathbf{n} \cdot \mathbf{D} = -\sigma_\Gamma, \qquad \mathbf{x} \in \Gamma_D, \tag{5.9}$$

where σ_Γ is the known surface density of electric charge, and usually, $\sigma_\Gamma = 0$. The subset Γ_φ is the union of $M+1$ regions $\Gamma_{\varphi j}$ ($j \in J_Q \cup J_V$, $J_Q = \{1,2,...,m\}$, $J_V = \{0,m,m+1,...,M\}$), that does not border on each other and are covered with infinitely thin electrodes. At these regions we set the following boundary for the electrical field conditions

$$\varphi = \Phi_j, \quad \mathbf{x} \in \Gamma_{\varphi j}, \quad j \in J_Q, \tag{5.10}$$

$$\int\limits_{\Gamma_{\varphi j}} \mathbf{n} \cdot \mathbf{D}\, d\Gamma = -Q_j, \quad I_j = \pm \dot{Q}_j, \qquad \mathbf{x} \in \Gamma_{\varphi j}, \quad j \in J_Q, \tag{5.11}$$

$$\varphi = V_j, \qquad \mathbf{x} \in \Gamma_{\varphi j}, \quad j \in J_V, \quad \Gamma_{j0} \neq \emptyset, \tag{5.12}$$

where the variables Φ_j, V_j do not depend on $\mathbf{x}$; Q_j is the overall electric charge on $\Gamma_{\varphi j}$, and the sign "$\pm$" in (5.11) is chosen in accordance with the accepted direction of the current I_j in the electric circuit. For magnetic boundary condition we suppose that on the boundary Γ hold the following condition

$$\mathbf{n} \cdot \mathbf{B} = 0, \qquad \mathbf{x} \in \Gamma. \tag{5.13}$$

For transient problems it is also necessary to pose initial conditions, which can be written as

$$\mathbf{u} = \mathbf{u}_*(\mathbf{x}), \quad \dot{\mathbf{u}} = \mathbf{v}_*(\mathbf{x}), \quad \varphi = \varphi_*(\mathbf{x}), \quad \phi = \phi_*(\mathbf{x}), \quad t = 0, \quad \mathbf{x} \in \Omega, \tag{5.14}$$

where $\mathbf{u}_*(\mathbf{x})$, $\mathbf{v}_*(\mathbf{x})$, $\varphi_*(\mathbf{x})$, $\phi_*(\mathbf{x})$ are the known initial values of the corresponding fields.

Equations (5.1)–(5.14) represent the statement of the transient problem for piezomagnetoelectric body with the generalized Rayleigh damping. We can also consider the particular cases of this model without tacking into account the connectivity between some physical fields (models of piezoelectric, piezomagnetic, and elastic materials).

5.3 Finite Element Approximations

For solving problems for the piezomagnetoelectric body in weak forms we will use classical finite element approximation techniques (Bathe and Wilson, 1976; Zienkewicz and Morgan, 1983). Let Ω_h be a region of the corresponding finite element mesh $\Omega_h \subseteq \Omega$, $\Omega_h = \cup_k \Omega^{ek}$, where Ω^{ek} is a separate finite element with number k. On the finite element mesh $\Omega_h = \cup_k \Omega^{ek}$ we will find the approximation to the weak solution $\{\mathbf{u}_h \approx \mathbf{u}, \varphi_h \approx \varphi, \phi_h \approx \phi\}$ for the transient problem in the form

$$\mathbf{u}_h(\mathbf{x},t) = \mathbf{N}_u^*(\mathbf{x}) \cdot \mathbf{U}(t), \quad \varphi_h(\mathbf{x},t) = \mathbf{N}_\varphi^*(\mathbf{x}) \cdot \boldsymbol{\Phi}(t), \quad \phi_h(\mathbf{x},t) = \mathbf{N}_\phi^*(\mathbf{x}) \cdot \mathbf{A}(t), \tag{5.15}$$

where $\mathbf{N}_u^*$ is the matrix of the shape functions for the displacements, $\mathbf{N}_\varphi^*$ is the row vector of the shape functions for the electric potential, $\mathbf{N}_\phi^*$ is the row vector of the shape functions for the magnetic potential, $\mathbf{U}(t)$, $\boldsymbol{\Phi}(t)$, $\mathbf{A}(t)$ are the global vectors of the nodal displacements, the electric potential, and the magnetic potential, respectively.

In accordance with conventional finite element technique we approximate the continuous weak formulation by the problem in finite-dimensional spaces. Substituting (5.15) and similar representations for project functions into the weak formulation of the problem for the magnetoelectric body on Ω_h, without taking into account the principal boundary conditions we obtain

$$\mathbf{M}_{uu} \cdot \ddot{\mathbf{U}} + \mathbf{C}_{uu} \cdot \dot{\mathbf{U}} + \mathbf{K}_{uu} \cdot \mathbf{U} + \mathbf{K}_{u\varphi} \cdot \boldsymbol{\Phi} + \mathbf{K}_{u\phi} \cdot \mathbf{A} = \mathbf{F}_u \,, \tag{5.16}$$

$$-\mathbf{K}_{u\varphi}^* \cdot (\mathbf{U} + \zeta_d \dot{\mathbf{U}}) + \mathbf{K}_{\varphi\varphi} \cdot \boldsymbol{\Phi} + \mathbf{K}_{\varphi\phi} \cdot \mathbf{A} = \mathbf{F}_\varphi + \zeta_d \mathbf{F}_\varphi^t \,, \tag{5.17}$$

$$-\mathbf{K}_{u\phi}^* \cdot (\mathbf{U} + \gamma_d \dot{\mathbf{U}}) + \mathbf{K}_{\varphi\phi}^* \cdot \boldsymbol{\Phi} + \mathbf{K}_{\phi\phi} \cdot \mathbf{A} = 0 \,, \tag{5.18}$$

with the initial conditions

$$\mathbf{U}(0) = \mathbf{U}_0, \quad \dot{\mathbf{U}}(0) = \mathbf{U}_0^t, \quad \boldsymbol{\Phi}(0) = \boldsymbol{\Phi}_0, \quad \mathbf{A}(0) = \mathbf{A}_0 \,, \tag{5.19}$$

where the vector of the nodal initial displacements $\mathbf{U}_0$, the vector of the nodal initial velocities $\mathbf{U}_0^t$, the vector of the nodal initial electric potentials $\boldsymbol{\Phi}_0$, and the vector of the nodal initial magnetic potentials $\mathbf{A}_0$ are derived from the corresponding continuous initial conditions (5.14).

Here, $\mathbf{M}_{uu} = \sum^a \mathbf{M}_{uu}^{ek}$, $\mathbf{C}_{uu} = \sum^a \mathbf{C}_{uu}^{ek}$, $\mathbf{K}_{uu} = \sum^a \mathbf{K}_{uu}^{ek}$, $\mathbf{K}_{u\varphi} = \sum^a \mathbf{K}_{u\varphi}^{ek}$, $\mathbf{K}_{u\phi} = \sum^a \mathbf{K}_{u\phi}^{ek}$ etc. are the global matrices, obtained from the assembly of the corresponding element matrices. The element matrices are provided in the following form:

$$\mathbf{M}_{uu}^{ek} = \int\limits_{\Omega^{ek}} \rho \mathbf{N}_u^e \cdot \mathbf{N}_u^{e*} \, d\Omega, \quad \mathbf{C}_{uu}^{ek} = \alpha_d \mathbf{M}_{uu}^{ek} + \beta_d \mathbf{K}_{uu}^{ek} \,, \tag{5.20}$$

$$\mathbf{K}_{uu}^{ek} = \int\limits_{\Omega^{ek}} \mathbf{B}_u^{e*} \cdot \mathbf{c} \cdot \mathbf{B}_u^e \, d\Omega, \quad \mathbf{K}_{u\varphi}^{ek} = \int\limits_{\Omega^{ek}} \mathbf{B}_u^{e*} \cdot \mathbf{e}^* \cdot \mathbf{B}_\varphi^e \, d\Omega \,, \tag{5.21}$$

$$\mathbf{K}_{\varphi\varphi}^{ek} = \int\limits_{\Omega^{ek}} \mathbf{B}_\varphi^{e*} \cdot \boldsymbol{\kappa} \cdot \mathbf{B}_\varphi^e \, d\Omega, \quad \mathbf{K}_{\varphi\phi}^{ek} = \int\limits_{\Omega^{ek}} \mathbf{B}_\varphi^{e*} \cdot \boldsymbol{\alpha} \cdot \mathbf{B}_\phi^e \, d\Omega \,, \tag{5.22}$$

$$\mathbf{K}_{\phi\phi}^{ek} = \int\limits_{\Omega^{ek}} \mathbf{B}_\phi^{e*} \cdot \boldsymbol{\mu} \cdot \mathbf{B}_\phi^e \, d\Omega, \quad \mathbf{B}_u^e = \mathbf{L}(\nabla) \cdot \mathbf{N}_u^{e*}, \quad \mathbf{B}_\varphi^e = \nabla \mathbf{N}_\varphi^{e*}, \quad \mathbf{B}_\phi^e = \nabla \mathbf{N}_\phi^{e*} \,, \tag{5.23}$$

where $\mathbf{N}_u^{e*}$, $\mathbf{N}_\varphi^{e*}$, $\mathbf{N}_\phi^{e*}$ are the matrices and the row vectors of approximate shape functions, respectively, defined on separate finite elements. The vectors $\mathbf{F}_u$, $\mathbf{F}_\varphi$, $\mathbf{F}_\varphi^t$ in (5.16), (5.17) are obtained from the boundary conditions, the corresponding right parts of the weak statements, and the finite element approximations.

Note that in ACELAN we use an effective algorithm for symmetric positive definite and quasi-definite matrices (Belokon et al, 2000, 2002; Nasedkin, 2010) for solving finite element Eqs. (5.16)–(5.18) (Benzi et al, 2005; Benzi and Wathen, 2008; Vanderbei, 1995). For example we can use the Newmark method for integrating Cauchy problem (5.16)–(5.19) with symmetric quasidefinite effective stiffness matrices in a formulation where the velocities and the accelerations at the time layers are not given explicitly (Belokon et al, 2002; Nasedkin, 2010). We can also implement in a symmetric form the most important procedures of finite element technologies such as the rotations of the degrees of freedom, the realizations of mechanical and electric boundary conditions, etc. ACELAN package also provides a two-dimensional version (Fig. 5.3) for non-homogeneously polarized materials.

5.4 Homogenization of Two-Phase Piezomagnetoelectric Materials

Let Ω be a representative volume of a two-phase composite heterogeneous body composed of two materials Ω_e and Ω_m ($\Omega = \Omega_e \cup \Omega_m$), where the phase Ω_e has the piezoelectric properties and the phase Ω_m has the piezomagnetic properties. Both phases Ω_e and Ω_m can consist of separate, generally speaking, disjointed subregions $\Omega_e = \cup_i \Omega_{ei}$, $\Omega_m = \cup_j \Omega_{ej}$, that in the aggregate have common boundaries and do not

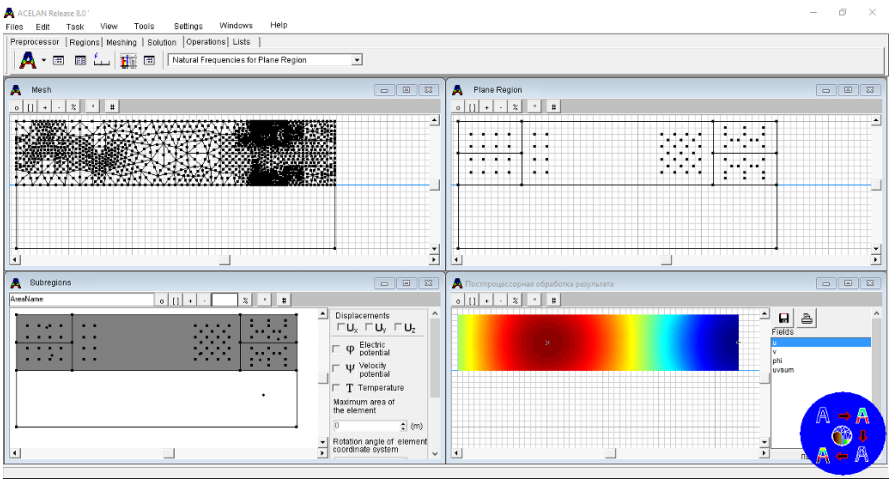

Fig. 5.3: 2D ACELAN package graphical user interface.

overlap each other. Thus, here we consider a two-phase mixture composite with piezoelectric and piezomagnetic fractions.

We assume that the both phases separately do not have magnetoelectric coupling. Then, for static homogenization problem we have the following system of equations

$$\mathbf{L}^*(\nabla)\cdot\mathbf{T}=0,\quad \nabla\cdot\mathbf{D}=0,\quad \nabla\cdot\mathbf{B}=0\,, \tag{5.24}$$

$$\mathbf{T}=\mathbf{c}\cdot\mathbf{S}-\mathbf{e}^*\cdot\mathbf{E}-\mathbf{h}^*\cdot\mathbf{H}, \tag{5.25}$$

$$\mathbf{D}=\mathbf{e}\cdot\mathbf{S}+\boldsymbol{\kappa}\cdot\mathbf{E}+\boldsymbol{\alpha}\cdot\mathbf{H}, \tag{5.26}$$

$$\mathbf{B}=\mathbf{h}\cdot\mathbf{S}+\boldsymbol{\alpha}^*\cdot\mathbf{E}+\boldsymbol{\mu}\cdot\mathbf{H}, \tag{5.27}$$

$$\mathbf{S}=\mathbf{L}(\nabla)\cdot\mathbf{u},\quad \mathbf{E}=-\nabla\varphi,\quad \mathbf{H}=-\nabla\phi\,, \tag{5.28}$$

where $\mathbf{c}=\mathbf{c}_a$, $\mathbf{e}=\mathbf{e}_a$, $\mathbf{h}=\mathbf{h}_a$, $\boldsymbol{\kappa}=\boldsymbol{\kappa}_a$, $\boldsymbol{\alpha}=\boldsymbol{\alpha}_a$, $\boldsymbol{\mu}=\boldsymbol{\mu}_a$ for $\mathbf{x}\in\Omega_a$, $a=e,m$.

We note that $\mathbf{e}_m=0$ and $\boldsymbol{\alpha}_m=0$ for $\mathbf{x}\in\Omega_m$, $\mathbf{h}_e=0$ and $\boldsymbol{\alpha}_e=0$ for $\mathbf{x}\in\Omega_e$, that is both phases separately do not have magnetoelectric coupling. However for composite magnetoelectric medium due to the coupling of the magnetic and mechanical fields at the piezomagnetic phase Ω_m and the coupling of the electric and mechanical fields at the piezoelectric phase Ω_e as the result we get the coupling of magnetic and electric fields that does not exist at each separate phase.

We will determine the effective moduli $\tilde{\mathbf{c}}$, $\tilde{\mathbf{e}}$, $\tilde{\mathbf{h}}$, $\tilde{\boldsymbol{\kappa}}$, $\tilde{\boldsymbol{\alpha}}$, $\tilde{\boldsymbol{\mu}}$ by the following technique (Nasedkin, 2014a,b) similarly for elastic and piezoelectric composites. Let us put some "equivalent" homogeneous piezomagnetoelectric medium Ω with the effective moduli $\tilde{\mathbf{c}}$, $\tilde{\mathbf{e}}$, $\tilde{\mathbf{h}}$, $\tilde{\boldsymbol{\kappa}}$, $\tilde{\boldsymbol{\alpha}}$, $\tilde{\boldsymbol{\mu}}$ into correspondence with initial heterogeneous medium. The constitutive equations for "equivalent" medium, similar to (5.25)–(5.27) for static problem, are given in the forms (with (5.28)):

$$\mathbf{T}=\tilde{\mathbf{c}}\cdot\mathbf{S}-\tilde{\mathbf{e}}^*\cdot\mathbf{E}-\tilde{\mathbf{h}}^*\cdot\mathbf{H}, \tag{5.29}$$

$$\mathbf{D}=\tilde{\mathbf{e}}\cdot\mathbf{S}+\tilde{\boldsymbol{\kappa}}\cdot\mathbf{E}+\tilde{\boldsymbol{\alpha}}\cdot\mathbf{H}, \tag{5.30}$$

$$\mathbf{B}=\tilde{\mathbf{h}}\cdot\mathbf{S}+\tilde{\boldsymbol{\alpha}}^*\cdot\mathbf{E}+\tilde{\boldsymbol{\mu}}\cdot\mathbf{H}. \tag{5.31}$$

We consider the static magnetoelectroelastic problems for representative volume with Eqs. (5.24)–(5.28) for composite medium and with Eqs. (5.24), (5.29)–(5.31), (5.28) for homogeneous medium, and with the following boundary conditions at the external boundary $\Gamma=\partial\Omega$

$$\mathbf{u}=\mathbf{L}^*(\mathbf{x})\cdot\mathbf{S}_0,\quad \varphi=-\mathbf{x}\cdot\mathbf{E}_0,\quad \phi=-\mathbf{x}\cdot\mathbf{H}_0,\qquad \mathbf{x}\in\Gamma, \tag{5.32}$$

where $\mathbf{S}_0 = \{\varepsilon_{011}, \varepsilon_{022}, \varepsilon_{033}, 2\varepsilon_{023}, 2\varepsilon_{013}, 2\varepsilon_{012}\}$; ε_{0ij} are some constant values that do not depend on $\mathbf{x}$; $\mathbf{E}_0$ and $\mathbf{H}_0$ are some constant vectors.

Thus, the static problem for an "equivalent" medium is the problem with the effective moduli. It is obvious that the solution of the problem (5.24), (5.29)–(5.31), (5.28), (5.32) has the following form: $\mathbf{u} = \mathbf{u}_0$, $\mathbf{u}_0 = \mathbf{L}^*(\mathbf{x}) \cdot \mathbf{S}_0$, $\varphi = \varphi_0$, $\varphi_0 = -\mathbf{x} \cdot \mathbf{E}_0$, $\phi = \phi_0$, $\phi_0 = -\mathbf{x} \cdot \mathbf{H}_0$, $\mathbf{S} = \mathbf{S}_0$, $\mathbf{E} = \mathbf{E}_0$, $\mathbf{H} = \mathbf{H}_0$, $\mathbf{T} = \mathbf{T}_0$, $\mathbf{T}_0 = \tilde{\mathbf{c}} \cdot \mathbf{S}_0 - \tilde{\mathbf{e}}^* \cdot \mathbf{E}_0 - \tilde{\mathbf{h}}^* \cdot \mathbf{H}_0$, $\mathbf{D} = \mathbf{D}_0$, $\mathbf{D}_0 = \tilde{\mathbf{e}} \cdot \mathbf{S}_0 + \tilde{\boldsymbol{\kappa}} \cdot \mathbf{E}_0 + \tilde{\boldsymbol{\alpha}} \cdot \mathbf{H}_0$, $\mathbf{B} = \mathbf{B}_0$, $\mathbf{B}_0 = \tilde{\mathbf{h}} \cdot \mathbf{S}_0 + \tilde{\boldsymbol{\alpha}}^* \cdot \mathbf{E}_0 + \tilde{\boldsymbol{\mu}} \cdot \mathbf{H}_0$.

From the solution of problem (5.24)–(5.28), (5.32) for a heterogeneous representative volume we find the fields $\boldsymbol{\varepsilon}$, $\mathbf{E}$, $\mathbf{H}$, $\boldsymbol{\sigma}$, $\mathbf{D}$ and $\mathbf{B}$. We note that for problem for a heterogeneous medium the equalities $\langle \boldsymbol{\varepsilon} \rangle = \boldsymbol{\varepsilon}_0$, $\langle \mathbf{E} \rangle = \mathbf{E}_0$ and $\langle \mathbf{H} \rangle = \mathbf{H}_0$ hold (Kurbatova et al, 2017; Nasedkin, 2014a,b; Nasedkin and Shevtsova, 2011), where the broken brackets denote the volume-averaged quantities

$$\langle (...) \rangle = \frac{1}{|\Omega|} \int\limits_{\Omega} (...) \, d\Omega. \tag{5.33}$$

For problem for the heterogeneous medium we accept the following equations for the determination of effective moduli: $\langle \mathbf{T} \rangle = \mathbf{T}_0$, $\langle \mathbf{D} \rangle = \mathbf{D}_0$, $\langle \mathbf{B} \rangle = \mathbf{B}_0$. Note that due to Kurbatova et al (2017); Nasedkin (2014a,b); Nasedkin and Shevtsova (2011) the average energies are equal for both heterogeneous and "equivalent" homogeneous piezomagnetoelectric media: $\langle \mathbf{T} \cdot \mathbf{S} + \mathbf{D} \cdot \mathbf{E} + \mathbf{B} \cdot \mathbf{H} \rangle / 2 = (\mathbf{T}_0 \cdot \mathbf{S}_0 + \mathbf{D}_0 \cdot \mathbf{E}_0 + \mathbf{B}_0 \cdot \mathbf{H}_0)/2$.

Now, by using Eqs. (5.32), we can select such boundary conditions, that enable us to obtain obvious expressions for the effective moduli. Indeed, setting in (5.32)

$$\mathbf{S}_0 = S_0 \mathbf{p}_\zeta, \quad \zeta = 1,2,...,6, \quad S_0 = \text{const}, \quad \mathbf{E}_0 = 0, \quad \mathbf{H}_0 = 0, \tag{5.34}$$

where ζ is fixed index ranging from 1 to 6; $\mathbf{p}_\zeta$ is the vector from six-dimensional basic set for the components of the strain tensor basic set; $\mathbf{p}_j = \mathbf{e}_j \mathbf{e}_j$, $j = 1,2,3$; $\mathbf{p}_4 = (\mathbf{e}_2 \mathbf{e}_3 + \mathbf{e}_3 \mathbf{e}_2)/2$; $\mathbf{p}_5 = (\mathbf{e}_1 \mathbf{e}_3 + \mathbf{e}_3 \mathbf{e}_1)/2$; $\mathbf{p}_6 = (\mathbf{e}_1 \mathbf{e}_2 + \mathbf{e}_2 \mathbf{e}_1)/2$; $\mathbf{e}_j$ are the basic vectors of the Cartesian coordinate system. From the solution of problem (5.24)–(5.28), (5.32), (5.34) we obtain the calculation formulas for the effective elastic stiffness moduli, piezoelectric moduli and piezomagnetic moduli:

$$\tilde{c}_{\beta\zeta} = \langle T_\beta \rangle / S_0, \; \beta = 1,...,6, \quad \tilde{e}_{j\zeta} = \langle D_j \rangle / S_0, \quad \tilde{h}_{j\zeta} = \langle B_j \rangle / S_0, \; j = 1,2,3. \tag{5.35}$$

If we assume that $E_0 = \text{const}$ in Eq. (5.32)

$$\mathbf{S}_0 = 0, \quad \mathbf{E}_0 = E_0 \mathbf{e}_m, \quad m = 1,2,3, \quad \mathbf{H}_0 = 0, \tag{5.36}$$

then from the solution of problem (5.24)–(5.28), (5.32), (5.36) we find the effective piezoelectric moduli, dielectric permittivity moduli and magnetoelectric coupling coefficients

$$\tilde{e}_{m\beta} = -\langle T_\beta \rangle / E_0, \; \beta = 1,2,...,6, \quad \tilde{\kappa}_{jm} = \langle D_j \rangle / E_0, \quad \tilde{\alpha}_{jm} = \langle B_j \rangle / E_0, \; j = 1,2,3. \tag{5.37}$$

If we assume that $H_0 = \text{const}$ in Eq. (5.32)

$$\mathbf{S}_0 = 0, \quad \mathbf{E}_0 = 0, \quad \mathbf{H}_0 = H_0 \mathbf{e}_l \quad l = 1,2,3, \tag{5.38}$$

then from the solution of problem (5.24)–(5.28), (5.32), (5.38) we find the effective piezomagnetic moduli, magnetoelectric coupling coefficients and magnetic permeability moduli

$$\tilde{h}_{l\beta} = -\langle T_\beta \rangle / H_0, \beta = 1,2,...,6, \quad \tilde{\alpha}_{jl} = \langle D_j \rangle / H_0, \quad \tilde{\mu}_{jl} = \langle B_j \rangle / H_0, \; j = 1,2,3\,. \tag{5.39}$$

Thus, we can find the full set of the effective moduli of piezomagnetoelectric composite mediim with arbitrary anisotropy class. For that we solve six problems (5.24)–(5.28), (5.32), (5.34), obtain the solutions of these problems, calculate the averaged by (5.33) mechanical stresses, electric flux densities, magnetic flux densities, and find the moduli from (5.35). Similarly, we solve three problems (5.24)–(5.28), (5.32), (5.36), obtain the solutions of these problems, and find the moduli from (5.37). Finally we solve three problems (5.24)–(5.28), (5.32), (5.38), obtain the solutions of these problems, and find the moduli from (5.39). Note, that the quantities $\langle T_\beta \rangle$, $\langle D_j \rangle$ and $\langle B_j \rangle$ in ((5.35), (5.37), (5.39) are different, since they are calculated from the solutions of the problems (5.24)–(5.28), (5.32) with different boundary conditions (5.32): (5.34), (5.36) and (5.38).

For the homogenization problems for two-phase piezomagnetoelectric composites in ACELAN-COMPOS package we can also use other less popular boundary conditions. Namely, instead of principal boundary conditions (5.32) with linear functions we can accept natural boundary conditions with constant quantities $\mathbf{T}_0$, $\mathbf{D}_0$ and $\mathbf{B}_0$

$$\mathbf{L}^*(\mathbf{n}) \cdot \mathbf{T} = \mathbf{L}^*(\mathbf{n}) \cdot \mathbf{T}_0, \quad \mathbf{n} \cdot \mathbf{D} = \mathbf{n} \cdot \mathbf{D}_0, \quad \mathbf{n} \cdot \mathbf{B} = \mathbf{n} \cdot \mathbf{B}_0, \qquad \mathbf{x} \in \Gamma, \tag{5.40}$$

and the mixed boundary conditions from (5.32), (5.40)

$$\mathbf{L}^*(\mathbf{n}) \cdot \mathbf{T} = \mathbf{L}^*(\mathbf{n}) \cdot \mathbf{T}_0, \quad \varphi = -\mathbf{x} \cdot \mathbf{E}_0, \quad \mathbf{n} \cdot \mathbf{B} = \mathbf{n} \cdot \mathbf{B}_0, \qquad \mathbf{x} \in \Gamma, \tag{5.41}$$

or

$$\mathbf{u} = \mathbf{L}^*(\mathbf{x}) \cdot \mathbf{S}_0, \quad \mathbf{n} \cdot \mathbf{D} = \mathbf{n} \cdot \mathbf{D}_0, \quad \mathbf{n} \cdot \mathbf{B} = \mathbf{n} \cdot \mathbf{B}_0, \qquad \mathbf{x} \in \Gamma, \tag{5.42}$$

or the other boundary conditions with use the relation $\phi = -\mathbf{x} \cdot \mathbf{H}_0$ instead of $\mathbf{n} \cdot \mathbf{B} = \mathbf{n} \cdot \mathbf{B}_0$ in (5.32), (5.40)–(5.42).

In ACELAN-COMPOS package we can also consider the particular cases of this model without taking into account the connectivity between some physical fields. For example, we can obtain the model of piezoelectric material, if we assume $\mathbf{h} = 0$, $\boldsymbol{\alpha}$ in (5.24), (5.25), and if we ignore the equations for magnetic fields.

5.5 Inhomogenious Polarization

The possibility to solve polarization definition problems in package ACELAN is based on the study by A.S. Skaliukh (Belokon and Skaliuh, 2010; Skaliukh et al, 2015; Soloviev et al, 2015). In this study a representative volume of polycrystalline

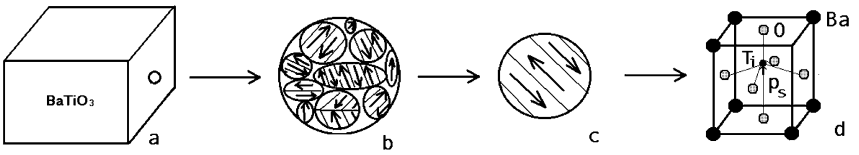

Fig. 5.4: Structure of perovskite-type polycrystalline ferroelectric material on example of barium titanate ceramic: a – ceramic sample; b – representative volume; c – dipoles in the crystallite; d – nuclear cell (Belokon and Skaliuh, 2010).

ferroelectric continuum which contains a great number of crystallites is analyzed. Each crystallite contains a great number of domains, and each domain has a set of cells with the same direction of spontaneous polarization, as shown in Fig. 5.4.

Each of the domains in the ferroelectric phase has the spontaneous polarization $\mathbf{p}_s$ and the spontaneous deformation ε_s, and one of the principal axes coincides with the direction of the spontaneous polarization. The domain switching process begins inside all crystallites when the electric field $\mathbf{E}$ is applied to the sample. All domains are arranged in a direction close to the direction of the electric field as the internal crystalline structure allows them. Fig. 5.5a shows a representative volume in the depolarized state, and Fig. 5.5b shows the pattern distribution of the domains after polarization. It was established experimentally that the domain switching begins only when the electric field reaches certain "threshold" values.

Numerical experiments were conducted with plain piezoelectric transducer (see Fig. 5.6) with stress free boundaries and with electrodes on upper and lower surfaces on the transducer. Material was PZT-4, the model included a study of damping with coefficients $\alpha = 2.7 \cdot 10^{-2}, \beta = \zeta = 3.84 \cdot 10^{-8}$. Length of the rod was 1 cm, its thickness changed in numerical experiments from 0.025 to 0.200 cm. Oscillations were excited by the voltage of 200 V.

The first part of the study consisted in analyzing mode shapes of the rod. In this research the longitudinal oscillations with coupled electro-mechanical fields were observed. We suggested that the polarization field corresponded to the strain field. This type of functions can be described as $F(x) = \sin(\pi k x/l)$, where l is the length of the rod. Effectiveness of piezoelectric device can be estimated by electro-mechanical coupling coefficient. We used the following representation:

Fig. 5.5 Direction of the vectors of spontaneous polarization in domains: a – before polarization; b – after polarization Belokon and Skaliuh (2010).

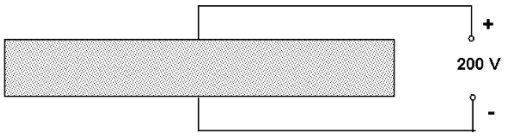

Fig. 5.6 Scheme of piezoelectric rod.

$$K^2 = \frac{f_a^2 - f_r^2}{f_a^2}, \tag{5.43}$$

where f_r is the resonance frequency and f_a is the antiresonance frequency. Some of observed polarization fields are present in Fig. 5.7.

Three resonance and antiresonance frequencies were analyzed for each case of polarization field. We estimated effectiveness of the transducer by comparing electro-mechanical coupling coefficient of the heterogeneously polarized specimen with a uniformly polarized one. Frequency differences between different cases were less than 5 %, but electro-mechanical coupling coefficient growth was large in some cases. For the first eigenmode no better scheme was found than the case of polarization field shown in Fig. 5.7 (top). Fig. 5.7 (middle) shows the most effective polarization field obtained for the second mode, and Fig. 5.7 (bottom) shows the best field for the third mode. In all cases the specimens of different thickness were analyzed.

In most cases the polarization of porous ceramics is considered as uniform over the body, directed along the applied electric field. However numerical experiments with finite element models in ACELAN package showed that in some cases these observation do not take place. Let us consider some example of the representative volumes. Top and bottom sides of the bodies have electrodes. Potentials applied to these electrodes creates polarization field in the material, transforming ceramics into

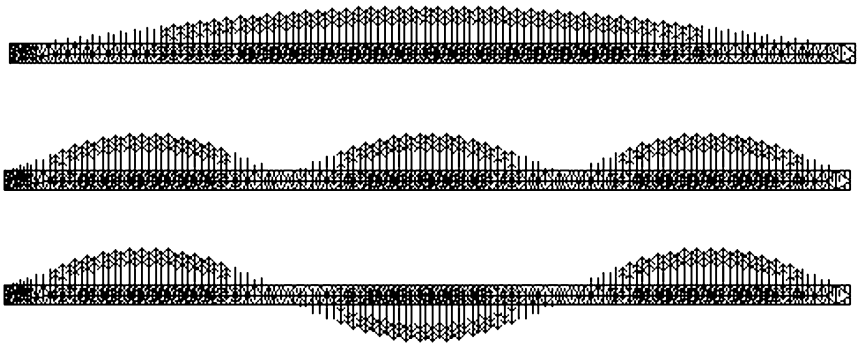

Fig. 5.7: Some inhomogeneous polarization fields.

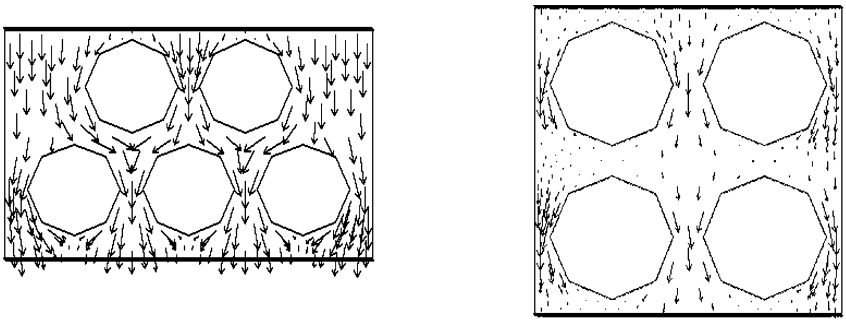

Fig. 5.8: Polorized porous ceramics with round pores.

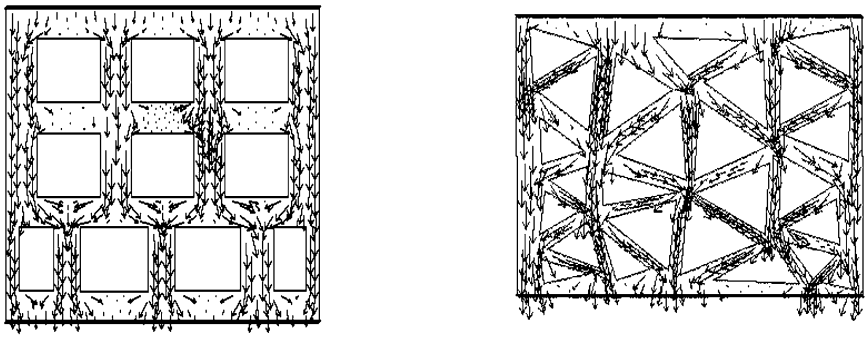

Fig. 5.9: Polorized porous ceramics with different types of pores.

piezoceramics. Pores are modeled as void areas without any material. Figures 5.8 and 5.9 shows examples of polarization field in bodies with different geometry and porosity percentage.

These models demonstrates that there are areas in the bodies where polarization direction is not the same with applied external field. In some areas there are no polarization at all. This fact has significant influence on piezoelectric properties of the bodies. Detailed study is presented in Vernigora et al (2011).

5.6 Three-Dimensional Models for Composite Materials

In 3D models the most common way to build a representative volume is to simulate a cube with predefined or randomized geometrical entities inside (Skaliukh et al, 2015). Representative volume technique is widely used in material science. Specialized module ACELAN-COMPOS consists of common finite element library, representative

volume generator and graphical user interface (GUI) for user interaction. The user has possibilities to choose among one of three basic two-phase models of material distribution in ACELAN package (Fig. 5.10): granules in the matrix, composites with two connected phases and rods (pillars) in the matrix. Each model is based on the enumeration algorithm which decides if the finite element belongs to material *A* or to material *B*.

ACELAN package was developed using .NET platform and C#. ACELAN has advanced program interfaces for exporting and importing models and meshes in .stl, .inp, .gmsh formats, and internal binary format developed for the package. ACELAN package has fully functional models for finite element analysis of generic meshes, but the main feature of new ACELAN-COMPOS package concern to design of active composites with tacking into account their internal structures.

In case of different types of materials in single composite (e.g. elastic and piezoelectric, piezomagnetic and piezoelectric, etc.) the number of degrees of freedom for each material can be different. This fact is taken into account during the assembly of global stiffness matrix to reduce its size.

Three algorithms were created to describe random material distribution for specific patterns: biphasic composite with connectivity of each phase, granules of predefined size, and rods of the second material in the matrix. Both patterns are inspired by well-known classes of composites: the first one can be classified as 3-3 or mixed (bulk) composite, the second one – as 3-0 composite, and last case as 3-1 composite (rods in polymer) in terms described by Newnham et al (1978).

Let us assume that the representative volume consists of clusters, each cluster consists of 512 equal cubes which are elements with regular distribution. Each cluster is randomly generated and placed in the representative volume. The number of clusters can vary from 1 to 8*n*, as far as we suggest that all clusters are of the

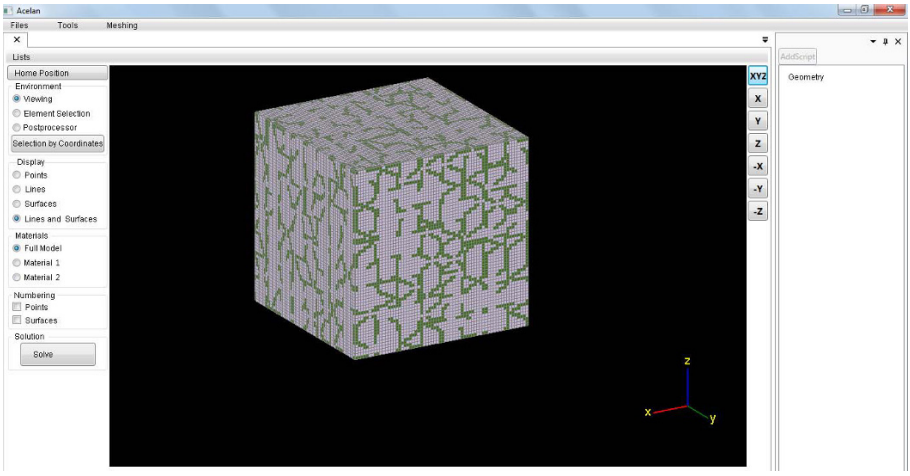

Fig. 5.10: 3D ACELAN package graphical user interface.

same size and the shape of the volume is predefined. The presented algorithms can be modified by changing assumptions about cluster size. Let's also state that the connectivity of material is a possibility to reach any element of the phase from any other element of the phase by passing through planes of elements. Connection of edges or nodes is not regarded as connectivity. Key point is considered as an element with predefined materials that cannot be changed. To make a random distribution of a biphasic composite made from materials A and B, we place 8 key points of the material A near each of the cube vertices and a starting point somewhere inside the cluster.

The connectivity of material B inside the cluster is guaranteed by the algorithm, the connectivity between clusters is achieved by adding 6 key points of material B, one for each external plane of cluster (Fig. 5.11). After that we make the shortest path between the starting point and the key point of the material A. The shortest path gives us about 15 % of the material A (Fig. 5.12). After that we add more elements to the path until the needed percentage reached.

The iterative process of adding new elements to the material A selects possible candidates on each step. The candidate element is an element that does not belong to the material A and can be removed from material B without disrupting the connectivity of the materials. Selecting such candidates is a basic problem of the graph theory. After the set of candidates is build, the algorithm randomly selects one candidate, adds it to the material A and starts the next iteration. A 2D example of a single step of this process is presented in Fig. 5.13. Examples of different representative volumes are shown in Fig. 5.14.

The described algorithm can be used independently in each part of the representative volume starting from $d = 4$. This fact allows us to use simple parallel computational techniques to increase the speed of numerical calculations. The sec-

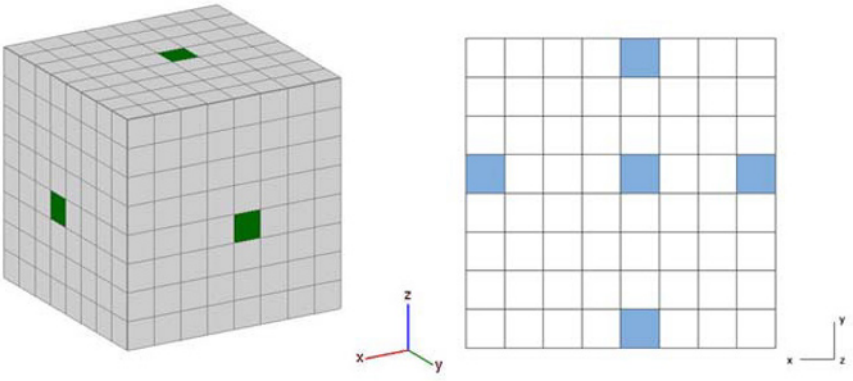

Fig. 5.11: Green elements represent material B, gray elements represent material A. The key points of the material B guarantee that the neighboring elements are connected by both phases.

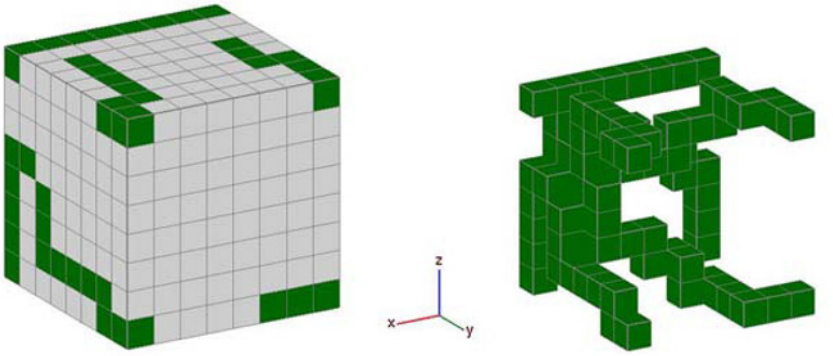

Fig. 5.12: Green elements represent material *A*, gray elements represent material *B*. Initial distribution (up to 15 % of material *A*).

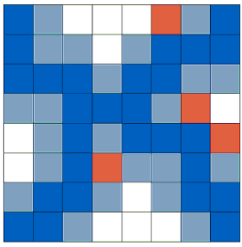

Fig. 5.13 The layer of the representative volume during some algorithm step of materials distribution. Dark blue color denotes the material *A*, light blue color denotes the candidates to be added to the material *A*, red color denotes the candidates that would disrupt the connectivity of the material *B* if added to *A*, and white denotes the material *B*.

ond algorithm is designed for the cases where material or pores are distributed in the form of isolated areas in the shape of granules. Granular composites are widely used in engineering and industry. As an example we consider granular composite polyester resin with the addition of calcium carbonate with mixtures of magnesium carbonate in the form of granules. The maximal and minimal sizes and overall percentage of granules can be set as input. On each step of iteration process, we select random key point in the cluster, with restriction that forbids the merging of granules (Fig. 5.15). Using this restriction, we select candidates for the next element to join the granule. There are up to six possible directions (Fig. 5.16) in which we can add new element. Random distribution for each candidate allows us to construct granules of natural form. 3D examples shown in Fig. 5.17.

The third type of representative volume contains rods placed in the skeleton of the main material. This is a straightforward algorithm based on placing 2D pattern on the bottom of the volume and extruding it through the body (Fig. 5.18).

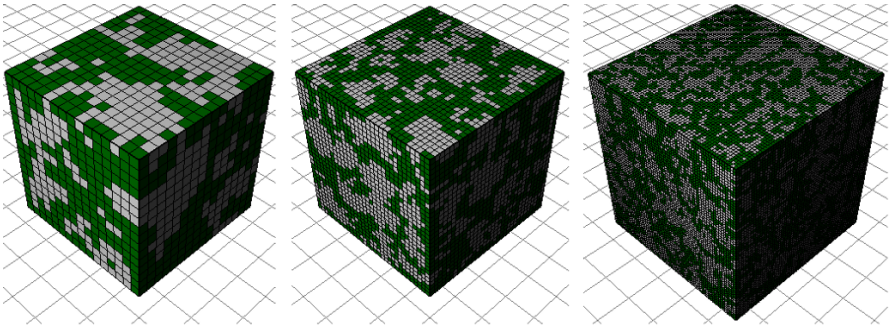

Fig. 5.14: Different representative volumes with two phases for composites of 3–3 connectivities.

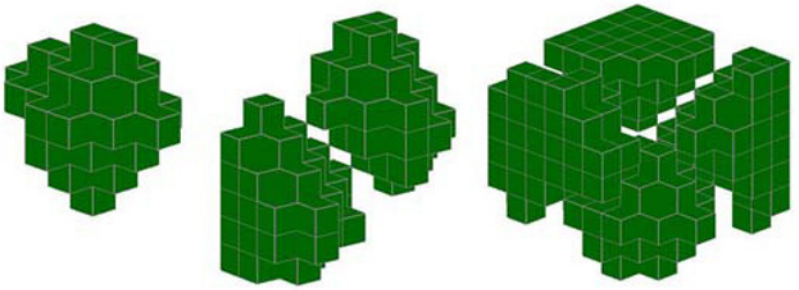

Fig. 5.15: Granules are distinguished by 1 element thick area.

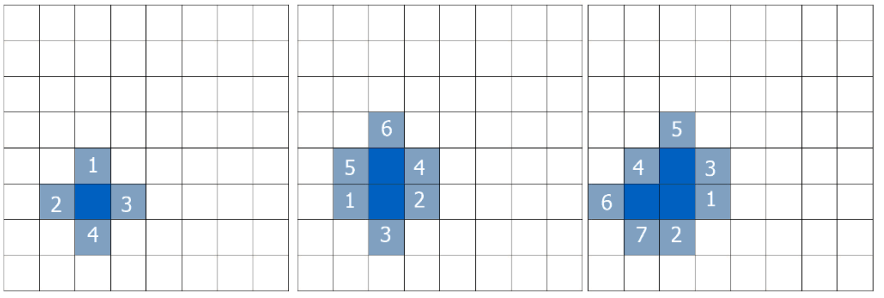

Fig. 5.16: Adding elements to the granule in 2D case.

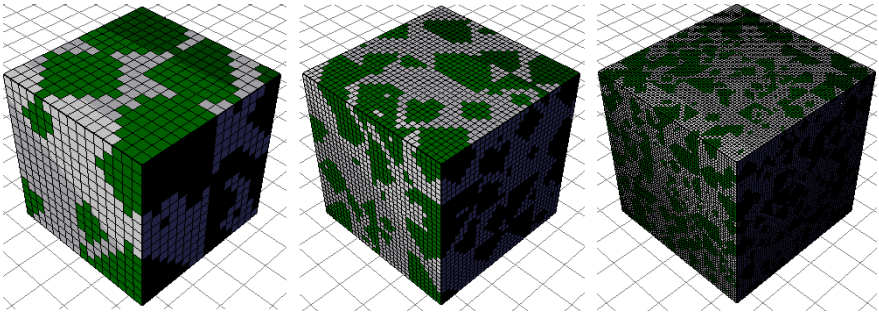

Fig. 5.17: Example: granular composite polyester resin with the addition of calcium carbonate with mixtures of magnesium carbonate in the form of granules. The maximal and minimal sizes and overall percentage of granules can be set as user input.

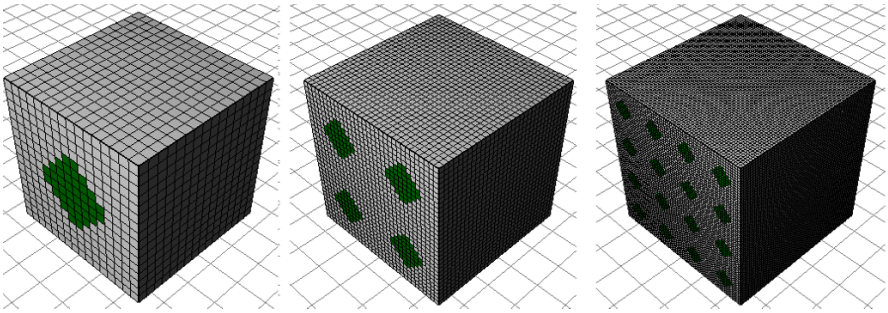

Fig. 5.18: Rods of different size in representative volumes with different meshes.

5.7 Conclusions

In the current paper we have described the models of active (piezomagnetoelectric and piezoelectric) composites and the possibilities of their simulation in the finite element software ACELAN and ACELAN-COMPOS.

The presented methods and programs are capable of solving the problems of definition of effective material characteristics for representative volumes with electroelastic and magnetoelastic properties. Both 2D and 3D cases we considered in the developed algorithms. Different types of the material distribution inside the representative volume were simulated in the mesh generating module. ACELANs program interfaces allows us to use generated meshes and models from external software packages and to use the imported meshes from other CAD/CAE software. ACELAN-COMPOS package allows us to determine the properties of two-phase active materials with 3–0, 3–3 and 3–1 connectivities.

Future possibilities of ACELAN-COMPOS package will be associated with the other types of the representative volumes and with the modeling of surface effects

and surface finite elements for piezoelectric and piezomagnetoelectric composite media on the micro- and nanoscale (Eremeyev and Nasedkin, 2017; Nasedkin, 2017).

Acknowledgements This work was supported by the Ministry of Education and Science of Russia, competitive part of state assignment, No. 9.1001.2017/PCh.

References

Bathe K, Wilson EL (1976) Numerical Methods in Finite Elements Analysis. Prentice-Hall, Englewood Cliffs, N

Belokon AV, Skaliuh AS (2010) Mathematical Modeling of Irreversible Processes of Polarization (in Russ.). FIZMATLIT, Moscow

Belokon AV, Eremeyev VA, Nasedkin AV, Solov'yev AN (2000) Partitioned schemes of the finite-element method for dynamic problems of acoustoelectroelasticity. Journal of Applied Mathematics and Mechanics 64(3):367–377

Belokon AV, Nasedkin AV, Solov'yev AN (2002) New schemes for the finite-element dynamic analysis of piezoelectric devices. Journal of Applied Mathematics and Mechanics 66(3):481–490

Benzi M, Wathen AJ (2008) Some preconditioning techniques for saddle point problems. In: Schilders WHA, van der Vorst HA, Rommes J (eds) Model Order Reduction: Theory, Research Aspects and Applications, Springer, Berlin, Heidelberg, Mathematics in Industry, vol 13, pp 195–211

Benzi M, Golub GH, Liesen J (2005) Numerical solution of saddle point problems. Acta Numerica 14:1–137

Bowen CR, Perry A, Kara H, Mahon SW (2001) Analytical modelling of 3-3 piezoelectric composites. Journal of the European Ceramic Society 21(10):1463–1467

Eremeyev VA, Nasedkin AV (2017) Mathematical models and finite element approaches for nanosized piezoelectric bodies with uncoulped and coupled surface effects. In: Sumbatyan MA (ed) Wave Dynamics and Composite Mechanics for Microstructured Materials and Metamaterials, Springer, Singapore, Advanced Structured Materials, vol 59, pp 1–18

Iyer S, Venkatesh TA (2014) Electromechanical response of (3-0,3-1) particulate, fibrous, and porous piezoelectric composites with anisotropic constituents: A model based on the homogenization method. International Journal of Solids and Structures 51(6):1221–1234

Kurbatova NV, Nadolin DK, Nasedkin AV, Nasedkina AA, Oganesyan PA, Skaliukh AS, Soloviev AN (2017) Mathematical models and finite element approaches for nanosized piezoelectric bodies with uncoulped and coupled surface effects. In: Sumbatyan MA (ed) Models of active bulk composites and new opportunities of ACELAN finite element package. In: Methods of wave dynamics and mechanics of composites for analysis of microstructured materials and metamaterials, Springer, Singapore, Advanced Structured Materials, vol 59, pp 133–158

Lee J, Boyd JG, Lagoudas DC (2005) Effective properties of three-phase electro-magneto-elastic composites. International Journal of Engineering Science 43(10):790–825

Li JY (2000) Magnetoelectroelastic multi-inclusion and inhomogeneity problems and their applications in composite materials. International Journal of Engineering Science 38(18):1993–2011

Martínez-Ayuso G, Friswell MI, Adhikari S, Khodaparast HH, Berger H (2017) Homogenization of porous piezoelectric materials. International Journal of Solids and Structures 113(Supplement C):218–229

Nan CW, Bichurin MI, Dong S, Viehland D, Srinivasan G (2008) Multiferroic magnetoelectric composites: Historical perspective, status, and future directions. Journal of Applied Physics 103(3):031,101

Nasedkin A (2014a) Modeling of magnetoelectric composites by effective moduli and finite element methods. theoretical approaches. Ferroelectrics 461(1):106–112

Nasedkin A (2017) Size-dependent models of multiferroic materials with surface effects. Ferroelectrics 509(1):57–63

Nasedkin AV (2010) Some finite element methods and algorithms for solving acousto-piezoelectric problems. In: Paronov IA (ed) Piezoceramic Materials and Devices, Nova Science Publ., NY, pp 177–218

Nasedkin AV (2014b) Multiscale computer design of piezomagnetoelectric mixture composite structures. AIP Conference Proceedings 1627(1):64–69

Nasedkin AV, Shevtsova MS (2011) Improved finite element approaches for modeling of porous piezocomposite materials with different connectivity. In: Paronov IA (ed) Ferroelectrics and Superconductors: Properties and Applications, Nova Science Publ., NY, pp 231–254

Nasedkin AV, Skaliukh AS, Soloviev AN (2014) New models of coupled active materials for finite element package ACELAN. AIP Conference Proceedings 1637(1):714–723

Newnham RE, Skinner DP, Cross LE (1978) Connectivity and piezoelectric-pyroelectric composites. Materials Research Bulletin 13(5):525–536

Nguyen BV, Challagulla KS, Venkatesh TA, Hadjiloizi DA, Georgiades AV (2016) Effects of porosity distribution and porosity piezoelectric foams. Smart Materials and Structures 25(12):125,028

Ramesh R, Kara H, Bowen CR (2005) Finite element modelling of dense and porous piezoceramic disc hydrophones. Ultrasonics 43(3):173–181

Ringgaard E, Lautzenhiser F, Bierregaard LM, Zawada T, Molz E (2015) Development of porous piezoceramics for medical and sensor applications. Materials 8(12):8877–8889

Rybyanets AN (2010) Ceramic piezocomposites: modeling, technology, characterization. In: Paronov IA (ed) Piezoceramic Materials and Devices, Nova Science Publ., NY, pp 115–174

Rybyanets AN (2011) Porous piezoceramics: theory, technology, and properties. IEEE Transactions on Ultrasonics, Ferroelectrics, and Frequency Control 58(7):1492–1507

Rybyanets AN, Nasedkin AV, Naumenko AA, Shvetsova NA, Lugovaya MA, Petrova EI (2015) Optimization of finite element models for porous ceramic piezoelements by piezoelectric resonance analysis method. In: Paronov IA, Chang SH, Theerakulpisut S (eds) Advanced Materials – Studies and Applications, Nova Science Publ., NY, pp 147–168

Skaliukh AS, Soloviev AN, Oganesyan PA (2015) Modeling of piezoelectric elements with inhomogeneous polarization in acelan. Ferroelectrics 483(1):95–101

Soloviev AN, Oganesyan PA, Skaliukh AS (2015) Modeling of piezoelectric elements with inhomogeneous polarization by using acelan. In: Paronov IA, Chang SH, Theerakulpisut S (eds) Advanced Materials – Studies and Applications, Nova Science Publ., NY, pp 169–192

Tang T, Yu W (2008) Variational asymptotic homogenization of heterogeneous electromagnetoelastic materials. International Journal of Engineering Science 46(8):741–757

Topolov VY, Bowen CR (2009) Electromechanical Properties in Composites Based on Ferroelectrics. Springer, London

Vanderbei RJ (1995) Symmetric quasidefinite matrices. SIAM Journal on Optimization 5(1):100–113

Vernigora GD, Lupeiko TG, Skaliukh AS, Soloviev AN (2011) About polazarition and effective properties identification for porous ceramics. DSTU Herald (Russ edition) 11(4 (55)):462–469

Zhang ZK, Soh AK (2005) Micromechanics predictions of the effective moduli of magnetoelectroelastic composite materials. European Journal of Mechanics - A/Solids 24(6):1054–1067

Zienkewicz OC, Morgan K (1983) Finite Elements and Approximation. John Wiley and Sons, N.Y.